

## Transient features of quantum open maps

Leonardo Ermann,<sup>1,\*</sup> Gabriel G. Carlo,<sup>1</sup> Juan M. Pedrosa,<sup>1,2</sup> and Marcos Saraceno<sup>1,2</sup>

<sup>1</sup>*Departamento de Física Teórica, GlyA, Comisión Nacional de Energía Atómica, Buenos Aires, Argentina*

<sup>2</sup>*Escuela de Ciencia y Tecnología, Universidad Nacional de San Martín, San Martín, Buenos Aires, Argentina*

(Received 14 March 2012; published 6 June 2012)

We study families of open chaotic maps that classically share the same asymptotic properties—forward and backward trapped sets, repeller dimensions, and escape rate—but differ in their short time behavior. When these maps are quantized we find that the fine details of the distribution of resonances and the corresponding eigenfunctions are sensitive to the initial shape and size of the openings. We study phase space localization of the resonances with respect to the repeller and find strong delocalization effects when the area of the openings is smaller than  $\hbar$ .

DOI: [10.1103/PhysRevE.85.066204](https://doi.org/10.1103/PhysRevE.85.066204)

PACS number(s): 05.45.Mt, 03.65.Sq

### I. INTRODUCTION

The quantum treatment of scattering situations where the trapped set has a complex fractal structure has recently been the source of much attention, particularly with respect to the confirmation of the fractal Weyl law [1–3] hypothesis concerning the global distribution of long-lived resonances and their localization properties on the classical repeller [4–7]. The use of quantum maps to model these systems has been of paramount importance, allowing extensive numerical, and sometimes analytical, results.

A classical “closed” map  $\mathcal{B}$  is represented as a diffeomorphism on a symplectic manifold  $\Sigma$  [8]. Its open version  $\tilde{\mathcal{B}}$  can be defined restricting the phase space to  $V$  (a subset of  $\Sigma$ ), which means that trajectories outside of these regions escape. The associated classical repeller  $\mathcal{K}$  is defined as the set of trajectories that remain on  $V$  both in the past and the future for infinite times (i.e., the intersection of the backward and forward trapped set). If the closed map  $\mathcal{B}$  is chaotic, the dynamics of  $\tilde{\mathcal{B}}$  on the repeller is hyperbolic and complex, and the resulting  $\mathcal{K}$  has a fractal structure with noninteger dimension  $d$ . Also, an initially uniform probability distribution in phase space decays exponentially with the classical escape rate  $\gamma$ . These are asymptotic features of the map appearing as  $T \rightarrow \infty$  that are associated with the global distribution of resonances and how their number scales with  $\hbar$ . Note that given an open map we have a unique associated repeller, but the converse is not true. A given repeller can be related to a large set of open maps [e.g., for the same  $\mathcal{B}$ , the repellers given by  $V$  and  $V'' = \tilde{\mathcal{B}}(V)$  are the same].

When quantized, the evolution of these systems is nonunitary; there is a probability loss reflecting the classical loss of trajectories. The corresponding operators have right and left decaying nonorthogonal eigenfunctions with complex eigenvalues  $\lambda_j$ , also referred to as resonances. They fall inside the unit circle in the complex plane [ $|\lambda_j|^2 = \exp(-\Gamma_j) \leq 1$ ]. The exponent  $\Gamma_j \geq 0$  can be interpreted as the rate at which probability is lost and thus is called the (quantum) decay rate. The long-lived resonances are those with the lowest decay rates, and they are directly associated to the classical repeller

$\mathcal{K}$ . Their  $\Gamma_j$  are related to the classical escape rate  $\gamma$  in the generic case (see, however, Ref. [9]).

In this paper we study classical maps having the same repeller and escape rate but different openings, and their corresponding quantum counterparts, by means of the paradigmatic tri-baker map. How these differences affect the behavior of the resonances is a fundamental question. Moreover, this is a crucial step in order to understand and evaluate the performance of the semiclassical theory attempting to describe open maps [10]. Of the many ways to open a map that lead to the same repeller, we have found that two of them are the most important for this purpose, giving rise to two families of maps. Keeping the area of the opening constant (*shift* family) or letting it increase (*intersection* family) defines it and is the source of important dynamical differences during the first time steps (though the asymptotic decay rate is the same for both of them). In the first case, we have found that by just varying the shape of the opening, the behavior of the long-lived portion of the spectrum changes slightly, in a nontrivial fashion. In the second case, the quantum spectrum changes as a whole. Finally, the shift family allows the identification of a quantum phase transition in the localization of the resonances, for openings with areas smaller than  $\hbar$ .

In the following we describe the organization of this paper: In Sec. II we define the family of maps that we study and their quantizations. In Sec. III we analyze the properties of the spectrum and the corresponding set of eigenfunctions by means of different measures and a phase space distribution that is especially useful for open maps [11]. Finally, in Sec. IV we point out our concluding remarks.

### II. OPEN MAPS

Given a repeller  $\mathcal{K}$  there are many open maps that have it as the invariant set. We will take  $V_1$ , an opening in phase space, as the generator of all of these open maps with the same repeller. For simplicity, in our example (which follows), it will be taken as symmetric in  $q$  and  $p$  (invariant under  $q \leftrightarrow p$  exchange). Other choices that do not respect this symmetry (or equivalent ones in other cases) lead to more differences in the resonances whose study is out of the scope of the present paper [12]. The next step in the construction consists of performing the evolution of  $V_1$  under  $\mathcal{B}^t$ , which will be called  $V_t \equiv \mathcal{B}^{t-1}(V_1)$ . Finally, simple combinations of  $V_t$  for positive

\*ermann@tandar.cnea.gov.ar

and negative times allow the creation of open maps, which can be grouped into map families according to their properties, all of them sharing the same repeller  $\mathcal{K}$ . Moreover, the iteration of open maps  $\tilde{\mathcal{B}}^i$  can be used alternatively to build new maps corresponding to this invariant set.

We will focus on two families of maps that are essentially given by preserving the area of the opening for all of its members on one hand, or not preserving it on the other. These families are the most interesting since they allow us to understand the dependence of the quantum spectrum on the shape and the size of the opening, while keeping the repeller and asymptotic decay rate invariant. The members of the first family  $\tilde{\mathcal{B}}_k^s$  with  $k = 1, 2, \dots$ , which we call the shift family, are defined as one iteration of the closed map  $\mathcal{B}$  followed by the escape of trajectories outside the region  $V_k$ . In turn, the intersection family is defined as  $\tilde{\mathcal{B}}_k^i$  with  $k = 1, 2, \dots$ , where the allowed region this time is given by the intersection of regions until time  $k$ ,  $V_k \cap V_{k-1} \cap \dots \cap V_2 \cap V_1$ . For this family, the allowed region decreases for larger  $k$  members. Of course, for nontrivial  $\mathcal{B}$  and  $V_1$  all family members are different, though the first members of both families are exactly the same by definition ( $\tilde{\mathcal{B}}_1^s \equiv \tilde{\mathcal{B}}_1^i$ ).

### A. The tri-baker map

We have chosen the paradigmatic tri-baker map as the model for our studies. This is one of the simplest chaotic maps that can be easily described by a ternary Bernoulli shift, and where the openings can be done following stable and unstable manifold directions. The general open map is defined as the composition of the *closed* tri-baker transformation followed by a given opening. We will define both shift and intersection families generated by an initial allowed region  $V_1$  having two horizontal strips  $p \in [0, 1/3) \cup (2/3, 1)$ . The openings will be defined to be symmetrical in  $q$  and  $p$ , in such a way as to maintain the time reversal symmetry of the closed map as shown in the left panel of Fig. 1 ( $k = 1$ ).

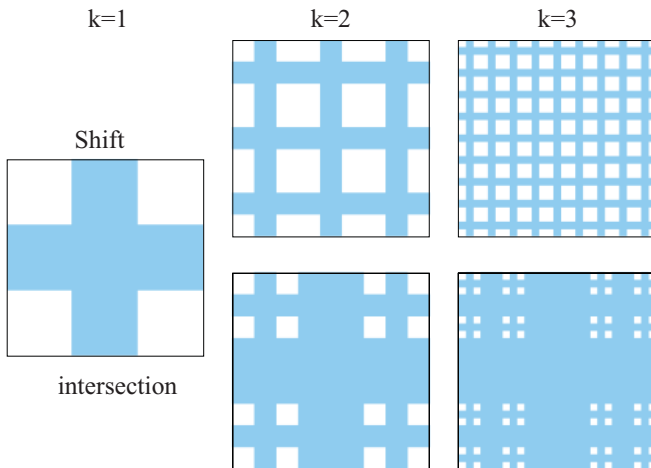


FIG. 1. (Color online) Phase space representation of the openings for shift and intersection families with  $k \leq 3$ , in top and bottom panels, respectively. The allowed regions are shown in white, while the corresponding openings are in light blue (gray).

The tri-baker map in a unit square phase space  $\mathbb{T}^2 \equiv [0, 1) \times [0, 1)$  is given by

$$\begin{pmatrix} q' \\ p' \end{pmatrix} = \mathcal{B} \begin{pmatrix} q \\ p \end{pmatrix} = \begin{pmatrix} 3q - [3q] \\ (p + [3q])/3 \end{pmatrix}, \quad (1)$$

where  $[q]$  denotes the integer part of  $q$ . The map is uniformly hyperbolic with Lyapunov exponent  $\lambda = \log 3$ . The symbolic notation of the map action is given by a Bernoulli shift in ternary representation of  $q = 0.\epsilon_0\epsilon_1\epsilon_2\dots$  and  $p = 0.\epsilon_{-1}\epsilon_{-2}\epsilon_{-3}\dots$  (given by the corresponding trits  $\epsilon_i = 0, 1, 2$ ) as

$$(\mathbf{p}|\mathbf{q}) = \dots\epsilon_{-2}\epsilon_{-1}\epsilon_0\epsilon_1\dots \xrightarrow{\mathcal{B}} (\mathbf{p}'|\mathbf{q}') = \dots\epsilon_{-2}\epsilon_{-1}\epsilon_0.\epsilon_1\dots, \quad (2)$$

where the dot is moved one position to the right. Different openings of both shift and intersection families can be straightforwardly defined in ternary notation using open trits  $\tilde{\epsilon}$  with forbidden value 1 ( $\tilde{\epsilon} = 0, 2$ ).

Shift family members  $\mathcal{B}_k^s$  have two open trits corresponding to the  $k$ th most significant trit of both position and momentum in ternary representation. On the other hand, intersection family members have the first  $k$  open trits of both position and momentum. In order to illustrate shift and intersection family members,  $\mathcal{B}_3^s$  and  $\mathcal{B}_3^i$  are shown in the next equations with open trits highlighted inside boxes:

$$\mathcal{B}_3^s \longrightarrow \dots\epsilon_{-5}\epsilon_{-4}\boxed{\tilde{\epsilon}_{-3}}\epsilon_{-2}\epsilon_{-1}\epsilon_0\epsilon_1\boxed{\tilde{\epsilon}_2}\epsilon_3\epsilon_4\dots, \quad (3)$$

$$\mathcal{B}_3^i \longrightarrow \dots\epsilon_{-5}\epsilon_{-4}\boxed{\tilde{\epsilon}_{-3}\tilde{\epsilon}_{-2}\tilde{\epsilon}_{-1}\tilde{\epsilon}_0\tilde{\epsilon}_1\tilde{\epsilon}_2}\epsilon_3\epsilon_4\dots. \quad (4)$$

The first three members of both families are represented geometrically in Fig. 1. In this way the classical escape rate can be computed analytically. When a closed trit is opened (transformation from  $\epsilon_j \rightarrow \tilde{\epsilon}_j$ ), the area of the allowed space is reduced by a factor of  $2/3$  ( $A \rightarrow 2/3A$ ).

For the case of the  $k$  member of the shift family, two trits are opened in the first iterations of the map until the first open trit of position ( $\epsilon_{k-1}$ ) reaches the  $k$ th most significant trit of momentum. From then on the map only opens one trit in each iteration. Therefore, during the first  $2k$  iterations the allowed area decreases by a factor of  $(2/3)^2$  in each step, and from then the area decreases by a factor of  $2/3$ . The same reasoning applies to the  $k$  member of the intersection family, where  $2k$  trits are opened in the first iteration, and from then only one closed trit is opened at each step. Therefore, the allowed area in the first step decreases suddenly by a factor of  $(2/3)^{2k}$ , but from the second step decreases by  $(2/3)$  and so on. Thus the asymptotic escape rate is the same for both families.

### 1. Quantum version

There are different ways to quantize the tri-baker map [13]. We will follow the Balazs-Voros-Saraceno (BVS) quantization, which is done by choosing antiperiodic boundary conditions in  $q$  and  $p$  [14]. The Hilbert space dimension is given by the integer  $D = 1/(2\pi\hbar)$  with position and momentum eigenvectors  $|q_j\rangle$  and  $|p_j\rangle$  (where  $j = 1, \dots, D$ ) connected by the antisymmetric Fourier transform  $G_D$ , given by

$$(G_D)_{j',j} \equiv \langle q_{j'}|p_j \rangle = \frac{1}{\sqrt{D}} e^{-i\frac{2\pi}{D}(j'+\frac{1}{2})(j+\frac{1}{2})}. \quad (5)$$

The quantum baker map on a Hilbert space of dimension  $D = 3M$  can be achieved converting the most significant qutrit of position in the most significant qutrit of momentum. The matrix of the map in mixed representation has the form of three diagonal blocks with a finite Fourier transform of size  $D/3$  in each one of them. In position representation we have

$$B_{\text{pos}} = G_D^\dagger B_{\text{mix}} = G_D^\dagger \begin{pmatrix} G_{D/3} & 0 & 0 \\ 0 & G_{D/3} & 0 \\ 0 & 0 & G_{D/3} \end{pmatrix}. \quad (6)$$

The map is opened by means of a projector  $\Pi$ , and in order to respect the  $q \rightleftharpoons p$  symmetry we will use quantum open maps of the form  $\tilde{B}_{\text{mix}} = \Pi B_{\text{mix}} \Pi$ .

The quantum version of the shift and intersection families can be easily implemented for the quantum tri-baker map on  $l$  qutrits with  $D = 3^l$ . The forbidden 1 in one trit  $\tilde{\epsilon}$  can be quantized by the one-qutrit projector  $\pi = I - |1\rangle\langle 1| = |0\rangle\langle 0| + |2\rangle\langle 2|$ . In this way, the projector applied to the  $i$ th qutrit can be written as

$$\Pi_i = \underbrace{I \otimes \cdots \otimes I}_{i-1} \otimes \pi \otimes \underbrace{I \otimes \cdots \otimes I}_{l-i} \quad (7)$$

with  $\Pi_i = \Pi_i^\dagger$ ,  $\Pi_i^2 = \Pi_i$ , and  $[\Pi_i, \Pi_j] = 0$ , where  $i, j = 1, \dots, l$ . Following this notation, the shift and intersection families of open quantum baker maps can be straightforwardly defined as

$$\tilde{B}_k^s = G_D^\dagger \Pi_k B_{\text{mix}} \Pi_k, \quad (8)$$

$$\tilde{B}_k^i = G_D^\dagger \Pi_1^\dagger \cdots \Pi_{k-1}^\dagger \Pi_k^\dagger B_{\text{mix}} \Pi_k \Pi_{k-1} \cdots \Pi_1, \quad (9)$$

with  $k = 1, \dots, l$ , respectively.

A phase space representation of the openings for the shift and intersection families with  $k \leq 3$  is shown in Fig. 1.

### III. RESULTS

#### A. Distribution of resonances

The quantum open maps  $\tilde{B}$  defined in Sec. II are represented by non-normal matrices of dimension  $D$  ( $[\tilde{B}, \tilde{B}^\dagger] \neq 0$ ). Therefore, their spectrum and eigenstates are given by

$$\tilde{B}|R_j\rangle = \lambda_j |R_j\rangle, \quad (10)$$

$$\langle L_j|\tilde{B} = \lambda_j \langle L_j|, \quad (11)$$

where the complex eigenvalues  $\lambda_j$  are inside unit circle  $|\lambda_j| \leq 1$  and  $|R_j\rangle$  and  $|L_j\rangle$  are the right and left eigenstates with  $j = 1, \dots, D$ . For a given eigenvalue, the corresponding left and right eigenstates are not equal in general, but they obey the orthogonality rule  $\langle L_j|R_{j'}\rangle \propto \delta_{j,j'}$ . In Fig. 2 we show the spectrum corresponding to both families. It can be seen that for the first member of each family the results are the same as we expected by definition. But for the last members allowed by the dimension  $D = 3^5 = 243$ , i.e.,  $k = 5$ , we find great differences. In fact, the one belonging to the shift family has a spectrum similar to the previous case while the one of the intersection family is highly contractive (it shrinks toward zero) due to the larger area of the openings.

In order to have a more detailed idea about the shape of the spectrum of both families, in Fig. 3 we show the

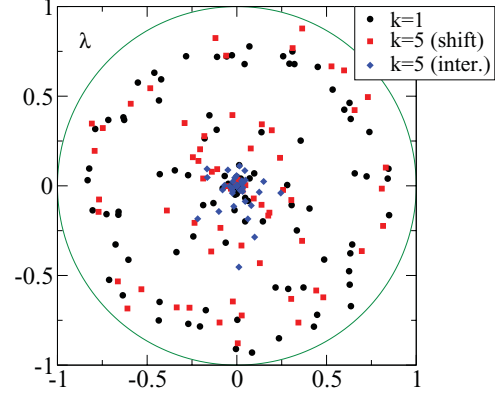


FIG. 2. (Color online) Spectrum in the complex plane for three different BVS quantum open baker maps with dimension  $D = 3^5 = 243$ . Black circles represent the eigenvalues for the first member of both the shift and intersection families ( $k = 1$ ), red (gray) squares stand for the shift family with  $k = 5$ , and blue (dark gray) diamonds stand for intersection with  $k = 5$ .

histograms corresponding to the distributions of the moduli of their eigenvalues for  $D = 3^7 = 2187$ .

It can be seen that the shift family has a nonmonotonic behavior with respect to the significance of the open trit. The long-lived sector of the resonances, clearly visible as a big bell toward the rightmost part of the histograms, “oscillates” from the right to left and back while more or less keeping its shape. This oscillation shows that although the classical escape rate is the same for all the maps, the average value of the decay rate of the long-lived states changes.

In the case of the intersection family there is a completely different behavior. At very short times (in fact, from the second time step on), the classical escape rate settles down to its asymptotic value. But the allowed area decreases suddenly also. This fact translates into the sudden shrinking of the spectrum as  $k$  increases. Indeed, the last member of this family allowed by the dimension  $D$  has all its eigenvalues heavily concentrated around modulus zero. For this specific case the decay rate of the first iteration of the map (i.e., the area of the opening) is related to the contraction of the longest-lived resonances. Then, it seems that one has to be aware of short time dynamics at the time of counting resonances, i.e., not only the escape rate and fractal dimension counts.

#### B. Eigenstates and the quantum repeller

We investigate the morphology of the eigenstates of the open tri-baker map families by making use of a recently introduced phase space representation suitable for open systems [11]. The first step is to define the symmetrical operators of right and left eigenstates,

$$\hat{h}_j = \frac{|R_j\rangle\langle L_j|}{\langle L_j|R_j\rangle}, \quad (12)$$

which are related to the eigenvalue  $\lambda_j$  and are independent from eigenstate normalization. These operators have the advantage that they clearly show the repeller structure underlying in the eigenstates. They are equivalent to projectors on the

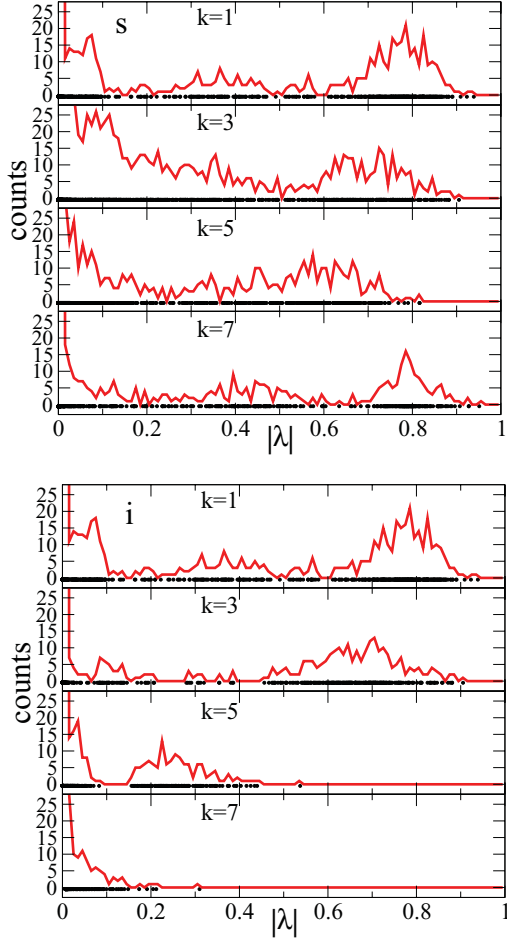


FIG. 3. (Color online) Distribution of resonances for shift (top panel) and intersection (bottom panel) quantum open baker maps with dimension  $D = 3^7 = 2187$ . Moduli of eigenvalues are represented by black circles for  $k = 1, 3, 5, 7$  from top to bottom, respectively. Histograms of these moduli for 100 intervals from 0 to 1 are shown by means of red (gray) lines.

eigenstates of unitary evolution operators. To have a better idea of how the set of long-lived resonances distribute on the classical repeller we also study the generalized operators onto this set taken as the sum of the first  $j$  of the  $\hat{h}_j$  projectors, ordered by decreasing modulus of the corresponding eigenvalues ( $|\lambda_j| \geq |\lambda_{j'}|$  with  $j \leq j'$ ):

$$\hat{Q}_j \equiv \sum_{j'=1}^j \hat{h}_{j'}. \quad (13)$$

From the definition of  $\hat{h}_j$  in Eq. (12) we have that  $\text{tr}(\hat{Q}_j) = j$  and  $\hat{Q}_j^2 = \hat{Q}_j$ , but  $\hat{Q}_j^\dagger \neq \hat{Q}_j$ .

The phase space representation of both  $\hat{h}$  and  $\hat{Q}$  operators can be defined by means of coherent states  $|q, p\rangle$  in the same way as in Ref. [11]:

$$h_j(q, p) = |\langle q, p | \hat{h}_j | q, p \rangle|, \quad (14)$$

$$Q_j(q, p) = |\langle q, p | \hat{Q}_j | q, p \rangle|. \quad (15)$$

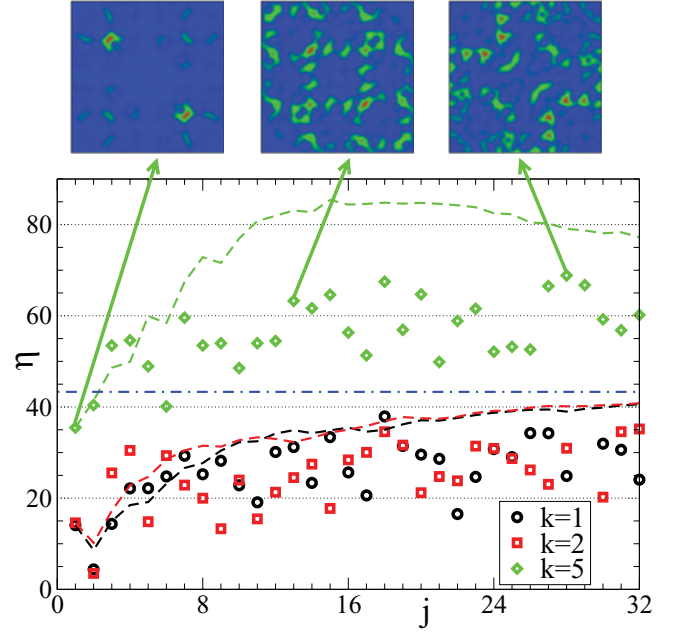


FIG. 4. (Color online) Norm ratio ( $\eta$ ) for  $\hat{h}_j$  operators of the *shift* quantum open baker maps with dimension  $D = 3^5 = 243$ . Black circles, red (gray) squares, and green (light gray) diamonds represent  $k = 1, k = 2$ , and  $k = 5$  members, respectively.  $\eta$  values for  $\hat{Q}_j$  with  $k = 1, k = 2$ , and  $k = 5$  are shown in black, red (gray), and green (light gray) dashed lines, respectively. Three Husimi functions ( $h_j(q, p) \equiv |\langle q, p | \hat{h}_j | q, p \rangle|$ ) for  $k = 5$  and  $j = 1, j = 13$ , and  $j = 28$  are shown going from zero [blue (dark gray)] to maximum value [red (gray)] on top panels (from left to right). The horizontal dot-dashed blue (dark gray) line is the norm ratio value obtained for the uniform quantum distribution on the repeller  $I_{\text{rep}}$ .

Clearly, the  $h_j$  and  $Q_j$  distributions tend to be localized on a discrete time version of the repeller (for Ehrenfest time  $l$ ). Individual  $h_j$  are distributed in the discrete time repeller in the same way as eigenstates of closed systems spread on the torus. It is worth mentioning that scarring phenomena are visible for some  $h_j$  on periodic orbits that belong to the repeller (see panels in Figs. 4 and 5).

In order to obtain a better characterization of the eigenstates we quantify the localization in phase space by defining the *norm ratio* ( $\eta$ ) of real and positive distributions  $h_j$  (and  $Q_j$ ):

$$\eta(h) = \left( \frac{\|h\|_1 / \|h\|_2}{\|\rho_c\|_1 / \|\rho_c\|_2} \right)^2, \quad (16)$$

where a coherent state is used for normalization  $\rho_c = |q, p\rangle \langle q, p|$  and the phase space norm is defined as

$$\|h\|_\gamma = \left( \int_{\mathbb{T}^2} h(q, p)^\gamma dq dp \right)^{\frac{1}{\gamma}}. \quad (17)$$

The norm ratio is independent of the  $h$  normalization and the position in phase space  $(q, p)$  of the coherent state in  $\rho_c$ . Note that the norm ratio is 1 for a coherent state by definition, and it reaches the maximum value  $D/2$  for a uniform distribution in a  $D$ -dimensional Hilbert space. For comparison purposes we define a uniform quantum distribution on the discrete version

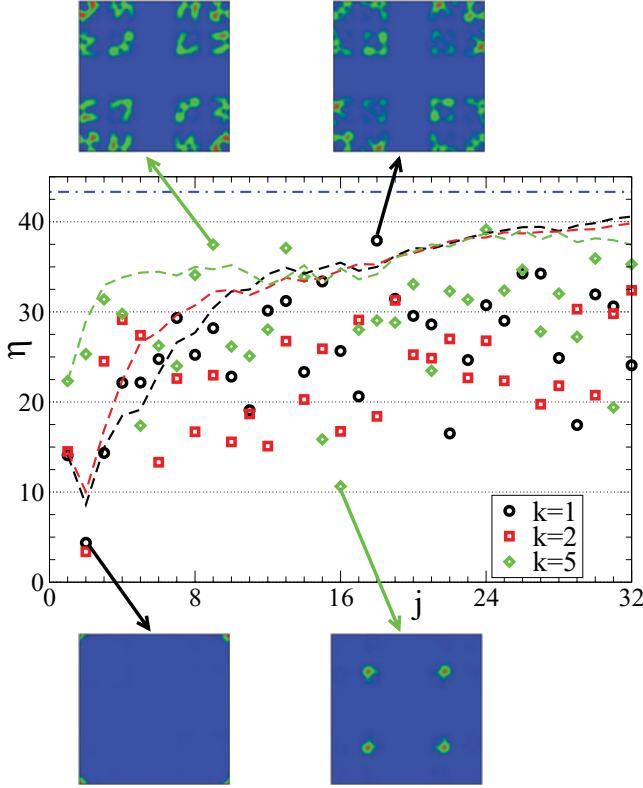


FIG. 5. (Color online) Norm ratio ( $\eta$ ) for  $\hat{h}_j$  operators of the intersection quantum open baker maps with dimension  $D = 3^5 = 243$ . Black circles, red (gray) squares, and green (light gray) diamonds represent  $k = 1, k = 2$ , and  $k = 5$  members, respectively.  $\eta$  values for  $\hat{Q}_j$  with  $k = 1, k = 2$ , and  $k = 5$  are shown in black, red (gray), and green (light gray) dashed lines, respectively. Four Husimi functions ( $h_j(q, p) \equiv |\langle q, p | \hat{h}_j | q, p \rangle|$ ) for  $k = 1$  and  $k = 5$  are shown going from zero [blue (dark gray)] to maximum [red (gray)]. The most localized cases corresponding to one periodic orbit scar ( $k = 1$  and  $j = 2$ ) and two periodic orbit scars ( $k = 5$  and  $j = 16$ ) are shown on the right and left bottom panels, respectively. Some cases of uniformly distributed functions on the repeller, for  $k = 5$  and  $j = 9$  and  $k = 1$  and  $j = 18$ , are illustrated on left and right top panels, respectively. The horizontal dot-dashed blue (dark gray) line is the norm ratio value obtained for the uniform quantum distribution on the repeller  $I_{\text{rep}}$ .

of the repeller as

$$I_{\text{rep}} = \sum_{j, j'}^D \chi_l(q_j, p_{j'}) |q_j, p_{j'}\rangle \langle q_j, p_{j'}|, \quad (18)$$

with  $j, j' = 1, \dots, D$ , and where  $\chi_l(q, p)$  is the finite time repeller defined as

$$\chi_l(q, p) = \begin{cases} 1 & \text{if } (q, p) \in \mathcal{K}_l \\ 0 & \text{otherwise} \end{cases} \quad (19)$$

with discrete time version of the repeller  $\mathcal{K}_l$  defined as the set of points that remain in the allowed region for the first  $l$  iterations (both for positive and negative times). The  $I_{\text{rep}}$  operator can be interpreted as the coherent state quantization of the finite time repeller (see Ref. [15]). The phase space representation for this operator,  $\langle q, p | I_{\text{rep}} | q, p \rangle$ , is shown in the top left panel of Fig. 6 for  $D = 3^5 = 243$ .

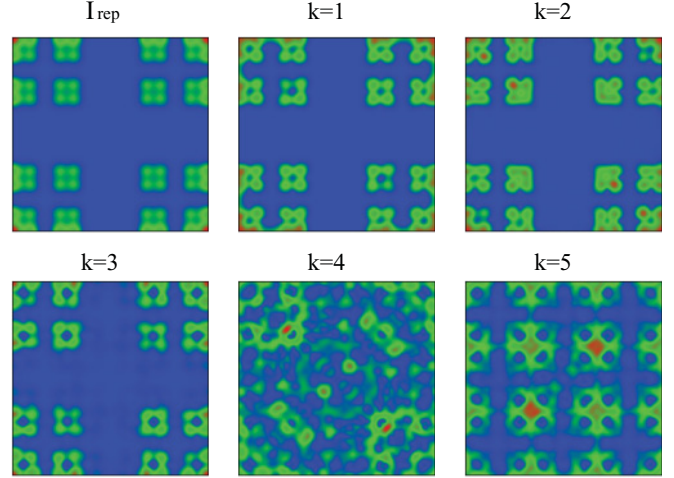


FIG. 6. (Color online) Phase space representation of  $\langle q, p | I_{\text{rep}} | q, p \rangle$  (left top panel) and  $Q_{32}$  operators for all members of the shift family with  $l = 5$ .  $Q$  functions are shown for  $k = 1, 2, 3, 4, 5$  and  $j = 2^5 = 32$  in a  $D$ -dimensional Hilbert space with  $D = 3^5 = 243$ . The values of the functions go from zero in blue (dark gray) to the maximum value in red (gray).

We have found that for the shift family the eigenstates corresponding to members having  $k \geq l/2$  (i.e., for which the openings have widths smaller or equal than  $\sqrt{\hbar}$ ) suddenly become strongly delocalized. By strong delocalization we mean that they show  $\eta$  values higher than the one corresponding to the  $I_{\text{rep}}$  distribution of Eq. (18), that is, the eigenstates are not only delocalized inside the discrete classical repeller but they have finite probability in classically forbidden regions in phase space. This can be clearly seen in Fig. 4, where the values of  $\eta$  are shown for the shift family members  $k = 1, 2, 3$ , for  $D = 3^5 = 243$ . The upper panels illustrate this remarkable behavior by means of phase space portraits (Husimi functions) of selected resonances. We should notice that for  $D = 3^5$  the families at  $k = 5$  imply openings of “pixel” size and thus generate strong diffraction. The  $Q$  distribution goes asymptotically toward the uniform distribution on the discrete version of the repeller for  $k < l/2$ , but clearly changes its behavior above this critical value. In this latter case the finite probability on forbidden regions of phase space is reflected by the  $\eta$  values of  $Q$  that saturate at about double that corresponding to the uniform quantum distribution on the discrete version of the repeller. Figure 6 shows the phase space representation of  $I_{\text{rep}}$  and  $Q_{32}$  for all members of the shift family ( $k = 1, 2, 3, 4, 5$ ).

On the other hand, the intersection family also shows an increase in  $\eta$  values for  $k \geq l/2$ , but this is now a very subtle effect (though a jump in  $\eta$  can be seen for  $Q$ ). All of its members have resonances distributed outside of the forbidden regions in phase space. They become more delocalized as  $k$  increases, but the  $\eta$  values always remain below the one corresponding to the uniform distribution on the discrete repeller. This is illustrated in Fig. 5 and its panels, which show phase space plots (Husimi functions) of selected resonances.

All of this is summarized in Fig. 7, where the average norm ratios, together with individual values for the resonances of

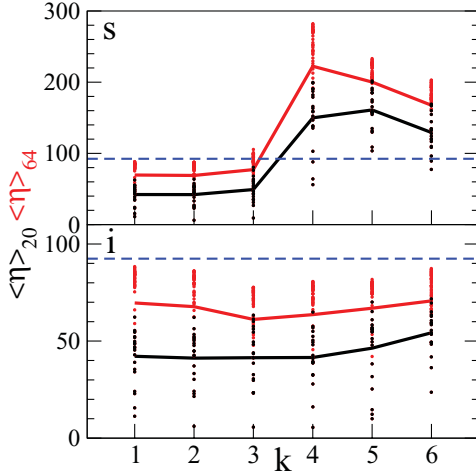


FIG. 7. (Color online) Average norm ratio  $\langle \eta \rangle$ , for both families of quantum open tri-baker maps for  $D = 3^6 = 729$ . Top and bottom panels show shift and intersection families, respectively. The average norm ratio for the first 20 and 64 eigenstates are shown in red (gray) and black lines, respectively. Black and red (gray) circles represent individual values of norm ratios for the first 20 eigenstates and for the next 42 eigenstates, respectively. The horizontal dashed blue (dark gray) line is the norm ratio value obtained for the uniform quantum distribution on the repeller  $I_{\text{rep}}$ .

both families, are shown (in this case we have taken  $D = 3^6 = 729$ ). It is clear that a quantum phase transition takes place at the level of the resonances of the shift family. The critical value of the parameter  $k$  is  $l/2$ , at which they become strongly delocalized and remain so for all values above it (we have confirmed this result for  $l \leq 9$ ). This applies to the long-lived portion of the spectrum as evidenced by the two limits taken in the corresponding average (i.e., for the first 20 and 64 eigenstates).

For the case of a given shift family member (fixed  $k > l/2$ ), the localization in the forbidden area disappears in the semiclassical limit (increasing  $l$ ), since  $k$  will be much smaller than the new  $l$  value. In the case of the intersection family there is no such phase transition, but the delocalization of the resonances slightly grows for  $k \geq l/2$ .

The main difference that exists for shift and intersection families is that for one map iteration, the allowed regions are distributed in the whole torus for the first case and only lay on the discrete time repeller for the second one (see Fig. 6). In the quantum case, for openings comparable with  $\hbar$ , the diffraction effects are very strong, leading to notably different behaviors between both families.

#### IV. CONCLUSIONS

We have investigated the behavior of the spectrum and the eigenstates corresponding to classical maps that share the same classical repeller (and other asymptotic properties), but differ in their short time behavior. Two families of these maps that we call *shift* and *intersection* play a significant role in understanding their dependence on the shape and the area of the escape region, respectively. We have found that there is a quantum phase transition in the resonances of the shift family. For openings having areas smaller than  $\hbar$

they become strongly delocalized in phase space, occupying forbidden regions. In previous works it has been demonstrated that for “classical” openings the resonance eigenfunctions are exponentially localized on the repeller [4–7]. Our results do not contradict this fact, as the higher  $k$  members of the shift family quickly reach situations in which the openings become “quantum,” naturally leading to strong diffraction, and to the subsequent delocalization in the forbidden region. The usual semiclassical theory does not account for these effects. Therefore, the quantum to classical link is nontrivial even at very short times. Correspondingly, for the shift family, the spectrum oscillates in a nontrivial way. The nature of the resonances for  $k \geq l/2$  is different from that corresponding to lower values of  $k$ , as can be seen from Fig. 7 (upper panel). This suggests that the oscillation in the spectrum does not reflect an equivalence of the long-lived sector of the extreme cases  $k = 1$  and  $l$ . This will be further investigated in Ref. [12]. In the case of the intersection family we have found no such phase transition. However, there is a growing delocalization of the states as  $k$  grows, and for  $k \geq l/2$  we have also identified a quick saturation of  $\eta$  values for both the eigenstates themselves and the  $Q$  distributions toward the uniform distribution on the discrete repeller. In this family, the effect of the intersection with wider openings erases the probability that escapes toward forbidden regions in phase space and this prevents the phase transition to occur here. The spectrum shrinks in this case, reflecting the sudden loss of probability due to a larger area of the opening as  $k$  grows.

All of this has very important consequences for the theory of open systems. First, we mention that the fractal Weyl law should take into account short time dynamics for any given dimension  $D$ , perhaps in its prefactor, and not only the invariants as the classical fractal dimension or escape rate. Also, the sensitivity of the spectrum with respect to which qubit is opened could have relevant implications to quantum computation. On the other hand, the strongly delocalized cases of the shift family pose an important question in order to understand the validity and performance of the semiclassical theory attempting to reproduce the spectrum and eigenstates of open maps. This is because this theory is based on highly localized functions, i.e., the so-called scar functions that are constructed with the classical information on and around the periodic orbits that live on the repeller. This lack of localization is probably due to the fact that for these extreme cases any quantum manifestation of the stable and unstable manifolds associated to the periodic orbits is lost. Then, it is crucial to understand how this phenomenon manifests itself even when the openings are not so extremely quantum in nature. This would not only give a better idea of how the semiclassical approximation works, but it would tell us its validity range and perhaps how we can improve it. Finally, open billiards constitute a very interesting field of application and verification of our findings [16,17]. Resonant microcavities for lasers can be adapted in order to realize the purely quantum repellers found for  $k \geq l/2$  [12].

#### ACKNOWLEDGMENTS

Partial support by ANPCyT and CONICET is gratefully acknowledged.

- [1] W. T. Lu, S. Sridhar, and M. Zworski, *Phys. Rev. Lett.* **91**, 154101 (2003).
- [2] H. Schomerus and J. Tworzydło, *Phys. Rev. Lett.* **93**, 154102 (2004).
- [3] S. Nonnenmacher and M. Zworski, *J. Phys. A* **38**, 10683 (2005).
- [4] J. P. Keating, M. Novaes, S. D. Prado, and M. Sieber, *Phys. Rev. Lett.* **97**, 150406 (2006).
- [5] J. P. Keating, S. Nonnenmacher, M. Novaes, and M. Sieber, *Nonlinearity* **21**, 2591 (2008).
- [6] J. Wiersig, *Phys. Rev. Lett.* **97**, 253901 (2006).
- [7] D. Wisniacki and G. G. Carlo, *Phys. Rev. E* **77**, 045201(R) (2008).
- [8] S. Nonnenmacher, *Nonlinearity* **24**, R123 (2011).
- [9] J. M. Pedrosa, G. G. Carlo, D. A. Wisniacki, and L. Ermann, *Phys. Rev. E* **79**, 016215 (2009).
- [10] M. Novaes, J. M. Pedrosa, D. Wisniacki, G. G. Carlo, and J. P. Keating, *Phys. Rev. E* **80**, 035202(R) (2009); J. M. Pedrosa, D. Wisniacki, G. G. Carlo, and M. Novaes, *ibid.* **85**, 036203 (2012).
- [11] L. Ermann, G. G. Carlo, and M. Saraceno, *Phys. Rev. Lett.* **103**, 054102 (2009).
- [12] L. Ermann and G. G. Carlo (unpublished).
- [13] L. Ermann and M. Saraceno, *Phys. Rev. E* **74**, 046205 (2006).
- [14] N. L. Balazs and A. Voros, *Ann. Phys.* **190**, 1 (1989); M. Saraceno, *ibid.* **199**, 37 (1990).
- [15] R. O. Vallejos and M. Saraceno, *J. Phys. A* **32**, 7273 (1999).
- [16] C. P. Dettman, *Frontiers in the Study of Chaotic Dynamical Systems with Open Problems*, edited by Z. Elhadj and J. C. Sprott, Chap. 11, World Scientist Series on Nonlinear Science, Series B, Vol. 16 (World Scientist, London, 2011).
- [17] J. Wiersig and J. Main, *Phys. Rev. E* **77**, 036205 (2008); S. Ree and L. E. Reichl, *ibid.* **65**, 055205(R) (2002).